EUROPEAN ORGANIZATION FOR NUCLEAR RESEARCH
CERN – ACCELERATORS AND TECHNOLOGY SECTOR

CERN-ATS-2013-022

Development of the EuCARD Nb_3Sn Dipole Magnet FRESCA2

P. Ferracin, M. Devaux, M. Durante, P. Fazilleau, P. Fessia, P. Manil, A. Milanese,
J. E. Munoz Garcia, L. Oberli, J. C. Perez, J. M. Rifflet, G. de Rijk, F. Rondeaux, E. Todesco

Abstract

The key objective of the Superconducting High Field Magnet work package of the European Project EuCARD, and specifically of the High Field Model task, is to design and fabricate the Nb3Sn dipole magnet FRESCA2. With an aperture of 100 mm and a target bore field of 13 T, the magnet is aimed at upgrading the FRESCA cable test facility at CERN. The design features four 1.5 m long double-layer coils wound with a 21 mm wide cable. The windings are contained in a support structure based on a 65 mm thick aluminum shell pre-tensioned with bladders. In order to qualify the assembly and loading procedure and to validate the finite element stress computations, the structure will be assembled around aluminum blocks, which replace the superconducting coils, and instrumented with strain gauges. In this paper, we report on the status of the assembly and we update on the progress on design and fabrication of tooling and coils.

Presented at ASC 2012
Applied Superconductivity Conference
October 7-12, 2012 – Portland, Oregon, US

Geneva, Switzerland
February 2013

Development of the EuCARD Nb_3Sn Dipole Magnet FRESCA2

P. Ferracin, M. Devaux, M. Durante, P. Fazilleau, P. Fessia, P. Manil, A. Milanese, J. E. Munoz Garcia, L. Oberli, J. C. Perez, J. M. Rifflet, G. de Rijk, F. Rondeaux, and E. Todesco

***Abstract*—The key objective of the Superconducting High Field Magnet work package of the European Project EuCARD, and specifically of the High Field Model task, is to design and fabricate the Nb_3Sn dipole magnet FRESCA2. With an aperture of 100 mm and a target bore field of 13 T, the magnet is aimed at upgrading the FRESCA cable test facility at CERN. The design features four 1.5 m long double-layer coils wound with a 21 mm wide cable. The windings are contained in a support structure based on a 65 mm thick aluminum shell pre-tensioned with bladders. In order to qualify the assembly and loading procedure and to validate the finite element stress computations, the structure will be assembled around aluminum blocks, which replace the superconducting coils, and instrumented with strain gauges. In this paper, we report on the status of the assembly and we update on the progress on design and fabrication of tooling and coils.**

***Index Terms*—Dipole magnet, Nb_3Sn, superconducting magnet, EuCARD.**

I. Introduction

The European Coordination for Accelerator R&D (EuCARD) Project was initiated in 2009 with the goal of carrying out research on new concepts and technologies for future upgrades of the European accelerators [1]. Among its activities, the Work Package 7 is dedicated to superconducting high field magnets for higher luminosities and energies. This work package has as key objective the fabrication and test of FRESCA2, a 100 mm aperture dipole generating a bore field of 13 T [2], [3]. The magnet, which will rely on Nb_3Sn superconductors, is aimed at upgrading the CERN cable test facility FRESCA [4], which uses Nb-Ti superconductors, bringing the bore field from 10 T to 13 T. In addition, it will provide the background field for an HTS insert [5].

This paper summarizes the status of the FRESCA2 magnet development, whose design was described in detail in [6]. We start presenting recent results on strand measurements and cable fabrication. The updated magnet parameters are then provided, as well as the status of coil and structure fabrication. We will then conclude with a description of the quench protection system and the future plans.

Manuscript received October 9, 2012. The research leading to these results has received funding from the European Commission under the FP7 Research Infrastructures project EuCARD, grant agreement no. 227579.

P. Ferracin, P. Fessia, A. Milanese, J. Munoz Garcia, L. Oberli, J. C. Perez, G. de Rijk, and E. Todesco are with CERN, CH-1211 Geneva 23, Switzerland (e-mail: paolo.ferracin@cern.ch).

M. Devaux, M. Durante, P. Fazilleau, P. Manil, J. M. Rifflet and F. Rondeaux are with CEA Saclay, 91191 Gif-sur-Yvette, France.

II. Conductor and Cable Parameters

The coils of FRESCA2 will be wound with a Rutherford cable composed of 40 strands with a diameter of 1 mm. Both a magnet unit length of Bruker Powder-in-tube (PIT) conductor, featuring 192 filaments, and a magnet unit length of OST Restacked-rod-process (RRP) conductor, with a 132/169 stack, have been ordered and are being delivered. Both conductors will be used to fabricate FRESCA2 coils. Parameters and properties provided in this paper refer to the PIT strand, whose qualification and characterization have been completed (Table I). Critical current measurements performed on virgin (round) strands and strands extracted from cables are shown in Fig. 1, where 4.2 K experimental data have been fitted by parameterization curves, extrapolated to 1.9 K, and compared to the magnet load-line. The measurements indicate that PIT virgin strands can reach a J_c in the superconductor of 2550 (1450) A/mm^2 at 12 (15) T and 4.2 K, including a self-field correction of 0.41 T/kA [7]. The heat treatment is optimized to obtain a RRR>150.

The final cable dimensions have been obtained as a result of a series of cabling tests, reported in [8]. With the final cable dimensions of 20.90 x 1.82 mm, the strands exhibit a cabling degradation of 5%. The cable will be insulated with braided S2™ glass yarn, with an assumed thickness of 0.200 mm.

For computation and tooling design purposes, the increase of cable cross-section during reaction has been taken into account: consistently with dimensional measurements performed on RRP strands and cables [9], a 2% and 4% increase have been applied respectively to the width and thickness of the cable.

TABLE I
Conductor and Cable Parameters

Parameter	Unit	
Strand diameter	mm	1
Fabrication process		PIT
Number of filaments		192
Effective filament diameter	μm	48
RRR		>150
Cu/SC		1.3
Jc (12 T, 4.2 K), with self-field correction	A/mm^2	2450
Jc (15 T, 4.2 K), with self-field correction	A/mm^2	1400
Number of strands		40
Cabling degradation	%	5
Cable bare width (before/after HT)	mm	20.90/21.32
Cable bare thickness (before/after HT)	mm	1.82/1.89
Transposition pitch	mm	120
Insulation thickness per side	mm	0.200
Cable unit length for coil 1/2	m	223/253

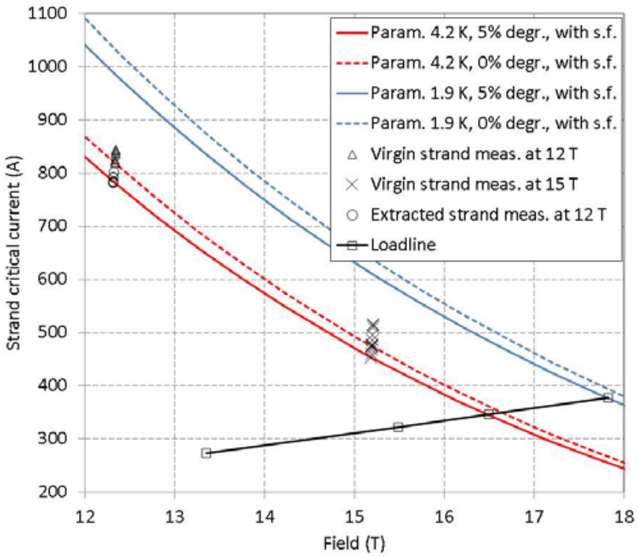

Fig. 1. Strand critical current (A) vs. magnetic field (T) measurements and parameterization curves of virgin strands (no degradation) and extracted strands (5% cabling degradation), together with magnet load-line.

In order to measure the cable length variation (along the longitudinal direction) during reaction, 1.5 m long samples of PIT cables were wound around winding poles, about 700 mm long and 90 mm wide, made of 3 different materials: iron, stainless steel, and titanium alloy (Fig. 2). For each material, two different winding configurations have been considered: a solid pole, with no gaps, and a segmented pole, with three axial gaps allowing the cable to contract. At the time of the submission of this paper, the first set of fixtures (Fig. 2, right) was heat treated. Further heat treatments with the other configurations and with RRP cable will follow.

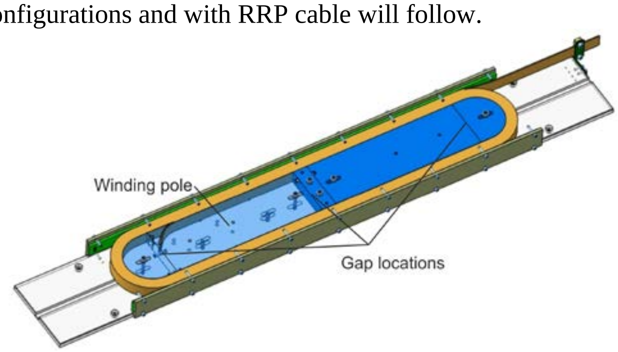

Fig. 2. Design of the fixture for the dilatation test.

III. Magnet Design and Parameters

The coil and magnet parameters are summarized in Table II. The coil-pack of FRESCA2 features two double-layer coils per quadrant (Fig. 3). Coil 1, closer to the mid-plane, is wound with 36 turns per layer (layer 1 and 2) around a Ti-alloy pole with a cut-out of 100 mm diameter and a minimum thickness of 8 mm. Coil 2, farther from the mid-plane, features 42 turns per layer (layer 3 and 4) wound around a solid iron pole. The coil lay-out was optimized to obtain a field homogeneity of <1% within 2/3 of the aperture. Each double-layer coil includes 0.5 mm thick fiber-glass insulation between the layers and two 300 μm thick insulated traces for quench protection on the external faces.

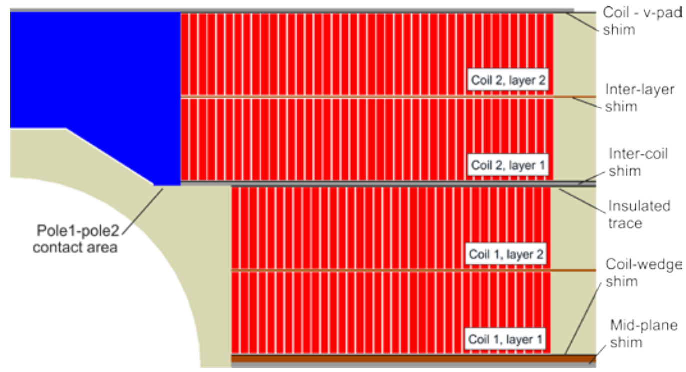

Fig. 3. Coil cross-section and insulation scheme (one quadrant at the centre of the straight section).

The inter-coil shims will be made by fiberglass sheets epoxy impregnated in-between the coils and mold-released, so to ensure uniform coil-to-coil contact, at the same time allowing detachment and replacement of individual coils.

In the end region, after a straight section of 728 mm, the cables are tilted up at 17^{o} angle, with a minimum cable "hard-way" bending radius of 700 mm at layer 4 (Fig 4, right). After the hard-way bends, the flared region features a short straight section of 24 mm in coil 1 and 32 mm in coil 2. The tilted ends are vertically supported by stainless steel wedges. The total coil length is 1.6 m. At the nominal bore field of 13 T, the conductor peak field of 13.4 T is located in the straight section of the pole turn in layer 1, the other layers having a field margin ranging from 1% in layer 2 to 9% in layer 4. In the nominal condition the magnet current will be 79% (72%) of the maximum "short-sample" current I_{ss} at 4.2 (1.9) K. The peak field in the end is 10% lower than in the straight section, and the 1% uniform field region is 540 mm long.

The support structure cross-section, depicted in Fig. 4 (left), follows a similar concept as the one adopted for the magnet HD2 [10]. It is characterized by an external aluminum shell 65 mm thick, two iron yoke halves, and vertical and horizontal pads surrounding the coils. Ten water pressurized bladders inserted between pads and yoke pre-tension the shell and compress the coil at room temperature. After cool-down, the coil is compressed to a maximum stress of -130 MPa, which prevents separation between pole and first turn at 13 T. The same principle is used in the end region, with 60 mm diameter aluminum rods compressing the coils by mean of 150 mm thick plates, thus minimizing the motions of the coil end blocks under the action of the axial electro-magnetic forces.

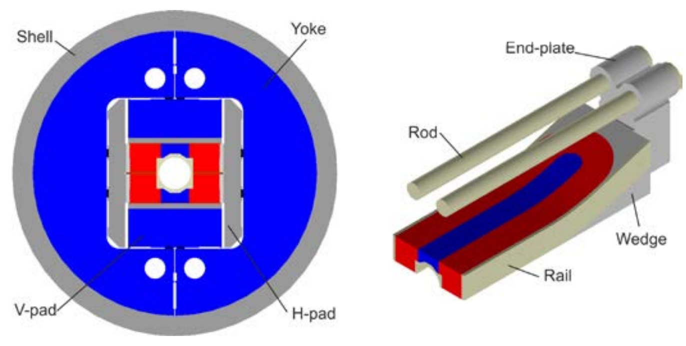

Fig. 4. Magnet cross-section (left) and view of ends with axial support (right).

TABLE II
COIL AND MAGNET PARAMETERS

Parameter	Unit	
Clear aperture diameter	mm	100
Magnet outer diameter	m	1.03
No. turns in layer 12/34 (quadrant)		36/42
Nominal bore field B_{nom}	T	13.0
Nominal current I_{nom}	kA	10.9
Conductor peak field at I_{nom}	T	13.4
Short sample current I_{ss} at 4.2/1.9 K	kA	13.8/15.1
Bore field at 4.2/1.9 K I_{ss}	T	16.0/17.2
Coil peak field at 4.2/1.9 K I_{ss}	T	16.5/17.8
Stored energy density in straight sect. at I_{nom}	MJ/m	3.8
Total stored energy at I_{nom}	MJ	4.6
Differential inductance at I_{nom}	mH/m	11.6
Fx / Fy coil 1 (per quadrant) at I_{nom}	MN/m	+3.4 / -0.5
Fz coil 1 (per octant) at I_{nom}	kN	200
Fx / Fy coil 2 (per quadrant) at I_{nom}	MN/m	+4.3 / -3.6
Fz coil 2 (per octant) at I_{nom}	kN	520

IV. STATUS OF COIL FABRICATION

The coil fabrication process follows three main stages: winding (with unreacted cable), heat treatment (or reaction) and instrumentation, and impregnation with epoxy resin. Each single double-pancake is fabricated separately, with two different sets of tooling. The challenges concerning the design and fabrication of the coil tooling are related to the high geometrical precision (±0.05 mm) requested for components up to 1.5 m long, the need of using the same coil parts from winding to magnet assembly, and the high temperature during reaction, which causes differential dilatation and metallurgic changes in the components. As a result, coil parts and tooling, currently either already produced or under fabrication, have been design simultaneously. Winding will be performed with the coil upside-down (Fig. 5, left). The top layer (i.e. 2 or 4) is wound on a tailored table, composed of three stainless steel blocks bolted together, starting from the layer jump splice. Once this first layer is wound and clamped to its target dimensions, the second layer (i.e. 1 or 3) is wound on top of it.

Most of the winding tooling parts are reused during reaction. Top plates and lateral shims are added around the coil in order to form a cavity, whose volume is defined according to the dimensions of the cable and their expected variations during heat treatment. Mica sheets are used between coil and plates to allow sliding during reaction.

After the heat treatment and the instrumentation of the coil external faces, the surrounding plates will be removed and replaced by the impregnation mould, made of aluminium and sealed (Fig. 5, right). Heating plates and thermocouples are used to control the impregnation (curing) temperature of 60 °C (125 °C). The whole tooling is put on an inclined plane and epoxy resin is injected from the bottom in a vacuum tank.

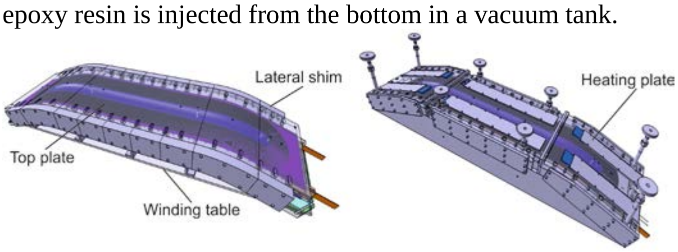

Fig. 5. Winding-reaction tooling (left) and impregnation tooling (right).

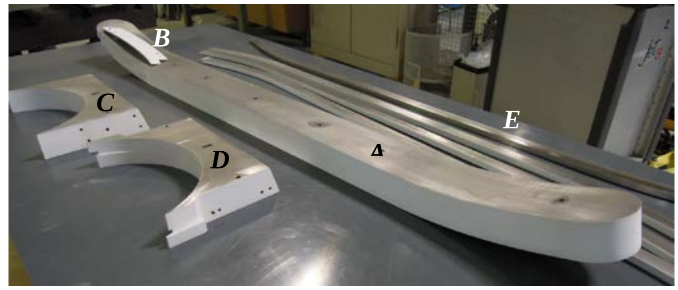

Fig. 6. Coil components after alumina deposition: central post (A), layer-jump shim (B), return-end end-shoe (C), lead-end end-shoe (D), side rails (E).

Each coil is wound from a continuous length of cable, so no internal splice is present. During magnet assembly, the coils are connected electrically in series by soldering Nb_3Sn leads to Nb-Ti cables: the operation is executed with copper pieces, which, after soldering with a 250 W electrical heaters, are used as thermal and mechanic stabilizer.

Coil components, shown in Fig. 6, follow all the coil fabrication steps. To enforce their mechanical rigidity, they are fabricated in one solid piece. An alumina layer of 300 μm is plasma-deposited on the surfaces facing the cable to provide an additional insulation layer. The fabrication process has been successfully tested on one qualification set: geometrical tolerances remain within ± 0.1 mm. Currently under study is the possibility to implement axial gaps in the central post to account for the cable length variations during reaction.

V. SUPPORT STRUCTURE FABRICATION AND ASSEMBLY

All the support structure components have been delivered. The 7075 aluminium alloy shell has been instrumented (Fig. 7, left) and placed around the yoke, composed of 5.8 mm thick iron lamination compressed by stainless steel end-plates. The vertical and horizontal pads have been bolted around aluminium "dummy" coils, which encompass poles, windings, rails, and end-shoes (Fig. 7, top right). Finally, Fig. 7 (bottom right) shows the axial support system, with four aluminium alloy rods bolted to two end-plates. A third plate together with an axial piston is used for room temperature pre-load.

Fig. 7. Aluminium shell, dummy coils, and axial support system.

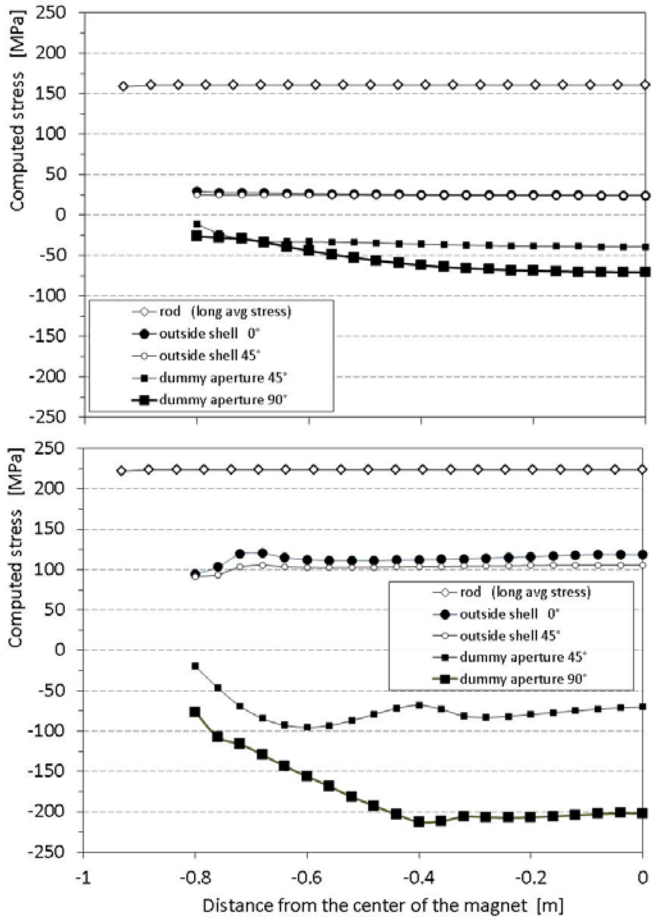

Fig. 8. Computed stress in outer shell (azimuthal), inner surface of dummy coil aperture (azimuthal) and axial rods (longitudinal) vs. *z* (along the bore axis) position, at room temperature (top) and after cool-down (bottom). Shell and dummy coils values are given at at 0°, 45°, and 90° from the mid-plane.

The outer diameter of the shell is instrumented with temperature-compensated half-bridge strain gauges, measuring both along the azimuthal and axial directions. The gauges are mounted on 10 stations distributed in the straight section and in the end regions, at 0° and 45° from the mid-plane. A similar gauge distribution is used on the inner radius of the aperture in the dummy coils. In addition, each axial rod is equipped with axial gauges mounted in opposite azimuthal locations to compensate bending effects. In total, 56 gauges were mounted.

Both 2D and 3D finite element models were implemented in ANSYS to analyse the structure mechanical behaviour. Fig. 8 shows the expected stresses at room temperature (top) and after cool-down (bottom) of the different components when assembled around the dummy coils. The data are plotted as a function of the axial position (along the bore axis), to point out the variations expected between straight section and ends. A friction coefficient of 0.2 was assumed between all surfaces in contact. The model indicates that in the nominal pre-load conditions, i.e. with shell and rod pre-tensioned to +25 MPa and +160 MPa respectively, the dummy coils will be compressed azimuthally to a stress of -70 MPa, decreasing to - 25 MPa in the ends. After cool-down, the shell and rod stress increase to +120 MPa and +220 MPa respectively, while the stress in the dummy coils will achieve a peak of -200 MPa in the straight section and -100 MPa in the ends.

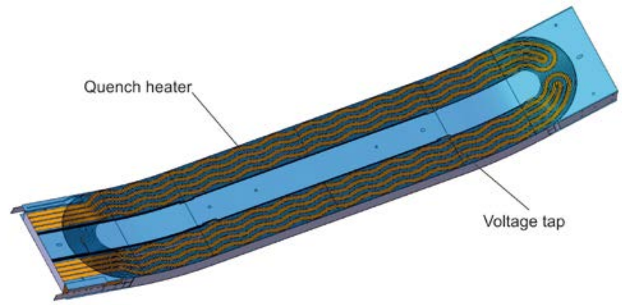

Fig. 9. Quench heater trace design.

The comparison between the model expectations and the strain gauge results obtained during a first assembly and cool-down to 77 K of the structure with dummy coils will allow a characterization of the structure mechanical behaviour, in particular in term of stress homogeneity and relation between shell/rod stress and coil stress.

VI. Quench Protection and Instrumentation

At nominal field, FRESCA2 has a total stored energy of 4.6 MJ, significantly larger than the ones of the Nb_3Sn dipoles and quadrupoles built in the last decade (for example, the 3.7 m long LARP long quadrupole magnet LQ features 1.4 MJ [11]). However, as pointed out in [12], the stored energy density in the coil is comparable to the other magnets. The quench protection system for FRESCA2 relies on a dump resistor and quench heaters. The value of the external resistor is 95 mΩ, set so that the voltage at the terminals of the magnet never exceeds 1 kV, ±500 V to ground by means of the grounding circuit. A 2D model implemented in CAST3M [13] has been used to determine the parameters of the quench protection system, under the assumption that quench heaters are placed on the outer surface of each layer, covering 50% of the total allowable surface and providing 50 W/cm² [14]. According to the computations, the detection time (from quench initiation to opening of the switch and activation of the heaters) must be lower than 40 (100) ms for a T_{max} below 150 (200) K in the high field region. The quench heaters design, shown in Fig. 9, is based on 25 μm thickness stainless steel strips with a 12 mm width. To cover the coil, whose width is 80 mm, we have two nested families of heaters, going from connection side to non-connection side and back, with a wiggling shape. The length of the heaters is 3.1 m, with a total surface per circuit of 370 cm^2, and a total resistance of 5.2 Ω. To get the required power, one needs 60 A, resulting in a voltage of 310 V at the end of each circuit.

VII. Conclusions and Future Plans

The status of the development of FRESCA2, a magnet aimed at upgrading the CERN FRESCA test facility, has been presented. With the measured strand properties, the magnet is capable of reaching the target bore field of 13 T operating at a current corresponding to 72% of the short-sample current at 1.9 K. All the structure components and the parts for the first coil have been delivered. In the coming months, the first coil is expected to be wound with a copper cable. In parallel, the support structure will be assembled, pre-loaded and cooled-down to 77 K around aluminium dummy coils.

REFERENCES

[1] http://eucard.web.cern.ch.

[2] G. de Rijk, "The EuCARD High Field Magnet Project," *IEEE Trans. Appl. Supercond.*, vol. 22, no. 3, 4301294, June 2012.

[3] L. Bottura, G. de Rijk, L. Rossi, and E. Todesco, "Advanced Accelerator Magnets for Upgrading the LHC," *IEEE Trans. Appl. Supercond.*, vol. 22, no. 3, 4002008, June 2012.

[4] D. Leroy, *et al.*, "Design and Manufacture of the Large-Bore 10 T Superconducting Dipole for the CERN Cable Test Facility," *IEEE Trans. Appl. Supercond*., vol. 10, no. 1, pp. 178-182, March. 2000.

[5] J.-M.G. Rey, *et al.*, "HTS Dipole Insert Development," *IEEE Trans. Appl. Supercond.* 23 submitted for publication.

[6] A. Milanese, *et al.*, "Design of the EuCARD High Field Model Dipole Magnet FRESCA2," *IEEE Trans. Appl. Supercond.*, vol. 22, no. 3, 4002604, June 2012.

[7] Bernardo Bordini, CERN, Geneva, Switzerland, private communication, 2012.

[8] L. Oberli, *et al*,, "Development of the Nb_3Sn Rutherford cable for the EuCARD high field dipole magnet FRESCA2," *IEEE Trans. Appl. Supercond.* 23 submitted for publication.

[9] H. Felice, *et al.*, "Impact of Coil Compaction on Nb_3Sn LARP HQ Magnet," *IEEE Trans. Appl. Supercond.*, vol. 22, no. 3, 4001904, June 2012.

[10] P. Ferracin, *et al*., "Recent Test Results of the High Field Nb_3Sn Dipole Magnet HD2", *IEEE Trans. Appl. Supercond*., vol. 20, no. 3, pp. 292-295, June. 2010.

[11] G. Ambrosio, *et al.*, "Test Results of the First 3.7 m Long Nb_3Sn Quadrupole by LARP and Future Plans," *IEEE Trans. Appl. Supercond.* vol. 21, no. 3, pp. 1858-1862, June 2012.

[12] E. Todesco, *et al.*, "Design studies for the low-beta quadrupoles for the LHC luminosity upgrade," *IEEE Trans. Appl. Supercond.* 23 submitted for publication.

[13] J.M. Fouet, P. Ladevèze, and R. Ohayon, *Calcul des structures et intelligence artificielle,* Pluralis, 1988, p. 261-271.

[14] H. Felice, *et al.*, "Instrumentation and Quench Protection for LARP Nb_3Sn Magnets," *IEEE Trans. Appl. Supercond.*, vol. 19, no. 3, pp. 2458-2461, June 2009.